Journal of
Mechanical
Science and
Technology

Journal of Mechanical Science and Technology 21 (2007) 1439~1444

Laser treatment of HVOF coating: model study and characterization

Z. Y. Taha-al[1], M. S. Hashmi[1], and B. S. Yilbas[2,*]

[1]*School of Mechanical and Manufacturing Engineering DCU, Dublin, Ireland*
[2]*ME Department, KFUPM, Dhahran, Saudi Arabia*

(Manuscript Received May 31, 2007; Revised August 30, 2007; Accepted September 30, 2007)

Abstract

HVOF coating is widely used in industry for protective coating of the metallic surfaces. The coating is based on the mechanical anchoring of the splats onto the substrate surface and thermal integration among the splats in the coating is not possible during the spraying process due to the operation temperature, which is lower than the melting temperature of the coating material. This, in turn, results in the formation of non-homogeneous structures and voids in the coating. One of the techniques to avoid such situations is to integrate the spats through the controlled melting. This can be achieved through the laser melting process. In the present study, laser melting of HVOF coating is modeled to determine the melt layer thickness. A lump parameter analysis is introduced in the model study and simulations are carried out in relation to the actual laser melting conditions. The melt layer predicted is compared with the experimental measurements. The microstructural analyses prior and post laser melting process are carried out using SEM and EDS. It is found that the predictions of the melt layer are in good agreement with experimental results.

Keywords: HVOF coating; laser meltingl SEM; EDS

1. Introduction

High velocity oxy-fuel (HVOF) coatings are widely used in industry for the wear applications and high temperature protection. The coating powder has resistance to high temperature and the abrasive operations, which enables the coating to be used in the power industry. Moreover, WC addition to the powder improves wear properties of the coating significantly. In HVOF coating process, the splats, semi-molten powder, anchors to the grit blasted surface through the mechanical locking. As the spraying progresses, the splats build up forming the coating layers. The particles during in-flight semi-molten state give rise to the formation of porous structures in the coating. This causes a non-homogeneous structure in the coating. Moreover, thermal integration of the splats in the coating reduces the porosity and improves the structural integrity in the coatings. This can be achieved through control melting of the coating. The laser melting process has several advantages over the conventional melting methods. The local heating resulting in small heat affected zone, precise operation, and fast processing time are the main advantages. The thermal strain developed during the heating and cooling cycles differs significantly in the coating. This, in turn, results in the development of the excessive stress field in the coating leading to the crack formation at the stress centers in the coating. Consequently, investigation of microstructural changes during the laser melting process becomes essential for possible structural integration in the coating.

Considerable research studies were carried out to examine HVOF coating and thermal processing. The Nd : YAG laser melting of nickel based superalloy coating was examined by Tuominen et al. [1]. They indicated that laser re-melting resulted in fully homo-

*Corresponding author. Tel.: +9663 860 4481, Fax.: +9663 860 2949
E-mail address: bsyilbas@kfupm.edu.sa

genization of the sprayed structure. Electron beam re-melting of HVOF sprayed alloys and carbides was investigated by Hamatoni and Miyazaki [2]. They showed that in order to reduce the number of pores and the unevenness of surface morphology, low fusing speed and homogeneous heating were preferable. Surface melting of thermally sprayed metallic coating was examined by Oksa et al. [3]. They showed that laser melted coatings had superior corrosion resistance in short term tests. Adhesion of thermally sprayed and laser deposited coatings was studied by Hjornhede and Nylund [4]. They indicated that laser coating had no delamination for strains upto 15%. The mechanical properties of laser treated HVOF coating was investigated by Yilbas et al. [5]. They observed that some locally distributed splats with high oxygen content were acted as crack initiation centers. Laser assisted spraying and laser treatment of thermally sprayed coating were examined by Suutala et al. [6]. They showed that the cracks perpendicular to the processing direction occurred when the Nd:YAG laser was used, however, this was diminished when the diode laser was used for re-melting process. Laser melting of thermally sprayed coating and microstructure changes in the melted zone were investigated by Kumari et al. [7]. They showed that microhardness increased by the post deposition treatment, but the extension of increase depended on the scanning speed as well as on the coating composition. Laser produced functionally graded tungsten carbide coatings were examined by Riabkina – Fishman et al. [8]. They indicated that the coating with 58% W provided wear resistance five times more than that of the untreated specimens. Laser treatment of HVOF coating and effects of treatment on the corrosion properties of the coating was examined by Tuomine et al. [9]. They showed that laser re-melting of coating improved the adhesion and homogeneity of the coating.

In the present study, laser re-melting of HVOF coating is considered and the microstructural analysis prior and post re-melting is carried out. Inconel is used as the spraying powder while stainless steel (SS 316L) is accommodated as the base material for spraying. EDS, optical microscopy and SEM are conducted for material characterization and micro-structural analyses. Laser heating situation is modeled using the lump parameter analysis and predications are compared with experimental findings.

2. Mathematical modeling of liquid layer formation

The lumped parameter technique can be used to formulate the liquid layer thickness during the laser heating process. In this case, it is assumed that the melt layer developed on the solid surface during laser irradiation flows steadily in the direction of the assisting gas due to the drag force developed at the assisting gas-liquid interface. Consider a small fraction (β) of molten metal evaporates from the melt surface during the laser heating process. Since the liquid layer thickness (δ_L) is formulated previously [10], the resulting equation is presented below:

$$\delta_L = \mu_L \frac{\sqrt{\frac{C_1}{C_5}s - \frac{5}{4}\frac{(C_4 + 2U_e^2)s}{C_5}}}{\frac{1}{2}C_f \rho_g U_e^2} \tag{1}$$

where

$$C_1 = \frac{1}{\rho_L}\frac{\frac{P_o}{A} + \dot{q}_c - h(T_m - T_{oi})}{[Cp_s(T_m - T_i) + L_m + \beta L_{ev} + 1.65Cp_m(T_{ev} - T_m)]}$$

and

$$C_2 = \rho_L[Cp_s(T_m - T_i) + L_m + \beta L_{ev} + 1.65Cp_m(T_{ev} - T_m)]$$

and

$$C_4 = \rho_g U_e C_H[Cp_g(T_{ev} - T_{oe})]$$

and

Table 1. Thermal properties used in the simulations for inconel 625 powder.

Source of Variation	Value	Units
Boiling temperature	3133	K
Melting temperature	1910	K
Density of assisting gas	1.97 at 150 kPa	kg/m³
Density of workpiece	8440	kg/m³
Fraction of evaporation contribution (β)	0.1	-
Specific heat capacity of solid	429	J/kgK
Specific heat capacity of melt	560	J/kgK
Specific heat capacity of gas	918	J/kgK
Thermal conductivity of molten metal	21.3	W/mK
Thermal conductivity of solid	9.8	W/mK
Latent heat of melting	10×2.72^5	J/kg
Latent heat of boiling	10×6.10^6	J/kg

$$C_5 = \frac{s}{2C_2} - \frac{1}{2}\mu_L \frac{1}{C_f \rho_g} \frac{2}{U_c^2}$$

A computer program is developed to compute the liquid layer thickness (δ_L) from Eq. (1) for various laser power settings. Table 1 gives the simulation conditions.

3. Experimental

The HVOF sprayed was carried out by (Applied Surface Technology Ltd.) using Diamond Jet Hybrid (DJ2600) of layer thickness of approximately 300 μm which were sectioned, mounted in resin and polished.

The CO_2 laser equipment used was Rofin DC 020 (Diffusion-cooled Slab CO_2). It has the properties of HF excitations with output power of 2000 W of power range from 200 to 2000 W. The beam quality factor for this equipment is to be considered as k > 0.9 and the pulse frequency is 0 or 2 up to 5000 Hz. The overlap tracks were performed on SS 316L sample plates through scanning the laser beam. The traverse speed of the samples varied from 10 to 150 mm/s. The spot size was changed from 1.2 mm to 0.6 mm. The mixture was pre-placed into the surface by means of thermal spray HVOF system. An overlap ratio of 0.4 was used to cover large areas. Argon was used as a shielding gas during processing to reduce oxidation of the Inconel 625 powder.

4. Results and discussion

Laser melting of HVOF sprayed Inconel 625 coating is studied and the melt layer thickness and microstructural changes in the laser re-melted zone are examined. The melt layer thickness is formulated using the lump parameter analysis and compared with the experimental results. Table 1 gives the thermal properties of the coating alloy used in the simulations.

Fig. 1 shows melt layers thickness with laser output power from predictions and experimental data. The melt layer thickness increases almost in a para-bolic form with increasing laser output power. In the analysis laser scanning speed and beam spot size at the workpiece surface are kept constant to resemble the experimental conditions. The non-linearity in the melt layer variation occurs for the laser power intensity ≤ 400 W. This is because of the heating situation during the formation of the melt layer at low laser power intensities. In this case, conduction and convection losses from the melt region are almost comparable to the laser power at low intensities. The increase in the conduction and convection losses from the melt site is incremental as the laser power increases. Consequently, increase in the melt size mostly depends on the increase in the laser irradiated power. This provides almost linear variation of melt layers thickness with increasing laser irradiated power beyond 400 W. When comparing the experimental results and predictions of melt layer thickness, it is evident that both results are in good agreement. Some small discrepancies between both results are because of assumptions of the structural homogeneity and porous free consideration as well as constant thermal properties used in the analysis. Although the porosity level in the coating is almost 2-3%, which is small, the oxide formation in the coating as a result of spraying process alters the thermal properties. In addition, thermal properties vary with temperature, provided that this variation is not significant. Consequently, the effects of structural changes such as oxide formation, and temperature dependent properties are responsible for the discrepancies between the experimental results and the predictions of the melt layer thickness.

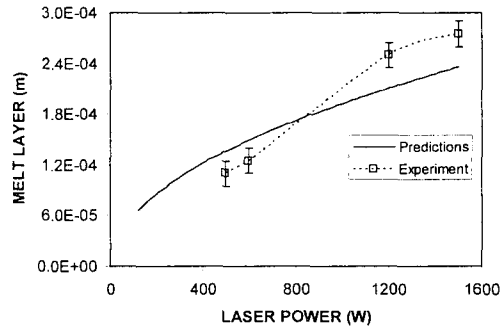

Fig. 1. Melt layer thickness with laser power predicted from the lump parameter analysis and obtained from the experiment.

Fig. 2 shows SEM micrographs of HVOF coating prior to laser melting. It can be observed that the coating consists of lamellar structure. The voids are scattered randomly provided that overall porosity is within 2-3%. Moreover, some oxidation around the splats is evident, which occurs during the in-flight prior to impacting the base material surface. Some dark inclusions around the splats are the evidence of brittle oxide particles. Fig. 3 shows SEM micrographs of the cross-section of laser melted and re-

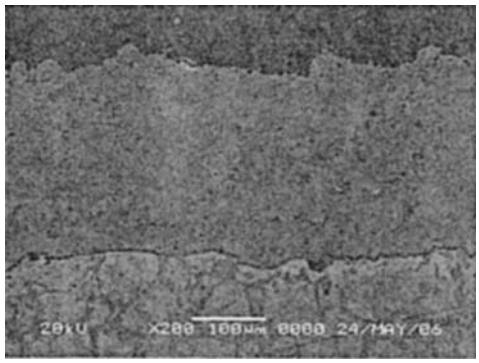

Fig. 2. SEM micrograph of HVOF coating cross-section prior to laser melting.

solidified coating structure. The coating material is Inconel 625 without WC inclusion. The cellular structure is observed upon solidification and the size of grain changes across the cross-section of the laser re-melted region. This is because of the non-uniform cooling at high rates. In this case, the liquid solution upon melting is solidified progressively while the composition of the solid is not uniform. The distribution of the solute in the solid after the completion of the solidification becomes different than from that in liquid. This situation is also observed from the EDS results (Table 2); in which case, non-uniformity of the elemental composition in the coating post laser re-melting is evident. Moreover, the development of transverse periodicity in the solidification process is also evident. This is attributed to the instability during the super-cooling process. In this case, cellular sub-structures are formed and then fine regular corrugated structures are developed extending along the regular cellular boundary. The corrugations are roughly parallel to the direction of growth of the crystal (Fig. 4). Furthermore, the formation of the cellular structure (Fig. 3) is because of the liquid, which is rapidly decanted exposing the solid-liquid interface. The cell size increases with decreasing rate of growth and the growth direction depends on the impurity content, speed of growth, and the inclination of the dendrite direction to the growth direction. The heat flow and cooling rate are related to the asymmetry in the shape of the cells, which in turn results in anisotropy of the growth rate of the cells. The segregation occurs at the grain boundaries during the process of solidification (Fig. 5), i.e. two crystals grow side-by-side and the boundary between them forms a groove. It should be noted that cellular segregation occurs when super-cooling takes place during the solidification. However,

Table 2. EDS results for the laser melted region. Each spectrum represents the different points across the cross-section of the coating after the laser treatment. The existing of gold in the spectrums is because of the gold coating of the samples prior to the EDS analysis.

Spectrum	C	Al	Cr	Fe	Ni	Au	Total
Spectrum 1		0.25	16.98	52.49	30.28		100.00
Spectrum 2	0.67		16.18	45.17	26.60	11.38	100.00
Spectrum 3	0.37		16.24	45.96	26.55	10.87	100.00
Spectrum 4	0.50		15.60	46.36	25.65	11.89	100.00
Spectrum 5	0.79		15.70	45.95	25.32	12.25	100.00
Spectrum 6	0.62		16.50	45.22	26.82	10.84	100.00
Spectrum 7	0.59		17.60	44.48	26.36	10.97	100.00
Spectrum 8	0.59		14.33	46.64	26.56	11.88	100.00
Spectrum 9	0.60		15.29	46.68	25.31	12.11	100.00
Max.	0.79	0.25	17.60	52.49	30.28	12.25	
Min.	0.37	0.25	14.33	44.48	25.31	10.84	

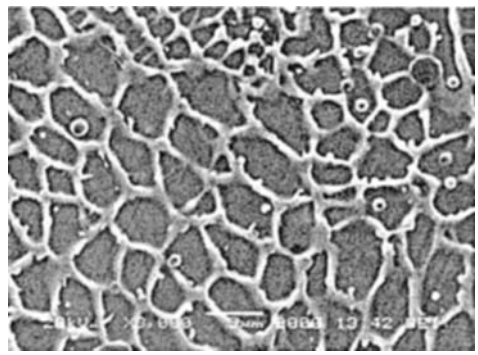

Fig. 3. SEM micrograph of laser HVOF coating cross-section after the laser treatment. The cellular structure is clearly observed.

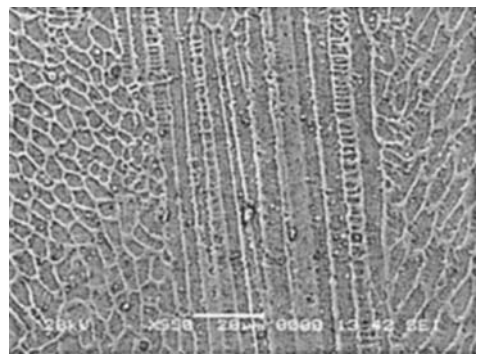

Fig. 4. SEM micrograph of laser HVOF coating cross-section after the laser treatment. The corrugations of the cellular structure are observed.

segregation degreases as a result of diffusion during the cooling after the solidification. In the cooling process, if the temperature gradient is reduced, then

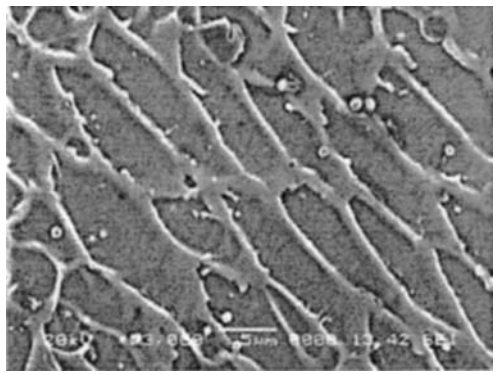

Fig. 5. SEM micrograph of laser HVOF coating cross-section after the laser treatment. The differences in the cell sizes are observed due to non-uniform cooling rates.

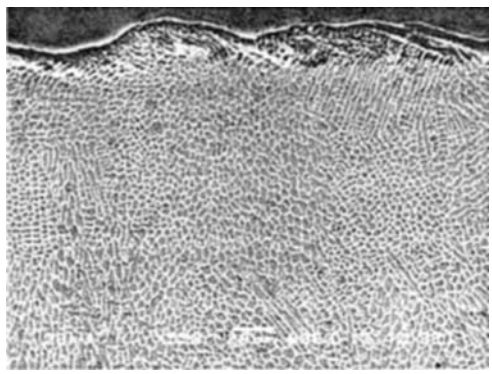

Fig. 6. SEM micrograph of laser HVOF coating cross-section after the laser treatment. The dendritic structure is observed in the surface region of the coating.

the zone of super-cooling extends. Consequently, the cells change to characteristic of dendrites forming cellular dendrites as seen from Fig. 6. This appearance is distinct from the cellular structure and free dendritic growth. One of the causes for this type of morphology is that the cellular dendritic type of growth occurs when the temperature gradient is small in the liquid phase providing the heat rejection into the solid at a low rate. Alignment of dendrites forms webs, which enhances conducting path for heat flow from the liquid to the crystals. It should be noted that the cellular-dendritic growth differs from cellular growth; in which case, the depth of super-cooled zone is greater for cellular growth.

5. Conclusion

HVOF sprayed and laser melted Inconel 625 coating is considered and metallurgical changes in the coating after laser re-melting process is examined. The melt layer thickness during laser irradiation of the coating is formulated using the lump parameter analysis. The predictions of melt layer thickness are compared with the experimental results. It is found that the predictions of liquid layer thickness agree with the experimental findings. However, some small discrepancies between in the results are attributed to the assumptions made in the analysis. In this case, the assumptions of homogeneous structure, constant thermal properties, and uniform laser heating situation are mainly responsible for these discrepancies. The re-crystallization of the laser melted layer results in cellular structure with different sizes. The change in the cell size is due to cooling rates, which are non-uniform in all directions. However, constitutional super-cooling causes the development of a transverse growth of cellular structure; in which case, elongated cellular structure is observed locally. The corrugations are almost parallel to the direction of growth of the crystals. Moreover, rapidly decanted liquid at the solid liquid interface results in almost uniformly distributed cellular structure. The free dendritic growth is observed locally, which is attributed to the extension of super-cooling due to locally reduced temperature gradient. The cellular type dendritic growth is also observed; in which case, temperature gradient in the liquid phase is small and latent heat of fusion is conducted into the solid.

Acknowledgment

The authors acknowledge the support of Dublin City University and King Fahd University of Petroleum and Minerals, Dhahran, Saudi Arabia for this work.

Nomenclature

A : Area (m^2)
Cp_g : Specific heat capacity of gas (J/kg.K)
Cp_m : Specific heat capacity of liquid (J/kg.K)
Cp_s : Specific heat capacity of solid (J/kg.K)
C_H : Heat transfer parameter
C_f : Skin friction coefficient
D : Diffision coefficient (m^2/s)
E_{in} : Laser power available at liquid surface (W)
$E_{Conduction}$: Rate of energy conducted (W)
$E_{Convection}$: Rate of energy convected (W)
E_{req} : Rate of energy required for melting (W)
H : Heat transfer coefficient (W/m^2K)

h_o : Total enthalpy of gas at the edge of the boundary layer (J/kgK)
h_g : Total enthalpy of gas at the melt surface (J/kgK)
k : Thermal conductivity (W/m.K)
L_m : Latent heat of melting (J/kg)
L_{ev} : Latent heat of evaporation (J/kg)
m_g : Assisting gas mass flow rate (kg/s)
m_L : Liquid mass flow rate (kg/s)
Pr : Prandtl number
P_o : Laser output power reaching the melt surface after reflection (W)
Re_L : Liquid layer Reynolds number
S : Distance along the workpiece surface (m)
Sc : Schimit number
T_{ev} : Boiling temperature (K)
T_m : Melting temperature (K)
T_{oi} : Initial temperature of the workpiece (K)
T_{oe} : Gas temperature at the edge of the boundary layer (K)
T_{ref} : Reference temperature
U_e : Gas velocity at the edge of the gas boundary layer (m/s)
U_L : Melt velocity (m/s)
U_{LS} : Melt velocity at the melt surface (m/s)
V_L : Melt velocity normal to the surface (m/s)
Y : Distance normal to the workpiece surface (m)

Greek

β : Evaporation factor , <1
η : Thermal efficiency
ρ_g : Density of assisting gas (kg/m³)
ρ_L : Density of molten metal (kg/m³)
ρ_s : Density of workpiece material (kg/m³)

References

[1] J. Tuominen, P. Vuoristo, T. Mantyla, M. Kylmalahti, J. Vihinen and P.H. Andersson, Properties of Nickel superalloy coatings as-sprayed and with Nd-YAG laser remelting, Proceedings of the International Thermal Spray Conference. (2000) 589-596.

[2] H. Hamatani and Y. Miyazaki, Optimization of an electron beam remelting of HVOF sprayed alloys and carbides, *Surface and Coatings Technology.* 154 (2002) 176-181.

[3] M. Oksa, E. Turunen and T. Varis, Sealing of thermally sprayed coatings, *Surface Engineering.* 20 (2004) 251-254.

[4] A. Hjornhede, A. Nylund, Adhesion testing of thermally sprayed and laser deposited coatings, *Surface and Coatings Technology.* 184 (2004) 208-218.

[5] B.S. Yilbas, A.F.M. Arif, M.A. and M.A. Gondal, HVOF coating and laser treatment: three-point bending tests, *Journal of Materials Processing Tech-nology.* 164-165 (2005) 954-957.

[6] J. Suutala, Tuominen, and P. Vuoristo, Laser-assisted spraying and laser treatment of thermally sprayed coatings, *Surface & Coatings Technology.* 201 (2006) 1981-1987.

[7] S. Kumari, A.S. Khanna and A. Gasser, The influence of laser glazing on morphology, composition and microhardness of thermal sprayed Ni-WC coatings, *Surface Engineering*–Proceedings of the 4th Interna-tional Surface Engineering Conference, 200 (2006) 128-135.

[8] M. Riabkina-Fishman, E. Rabkin, P. Levin, N. Frage, M.P. Dariel, A. Weisheit, R. Galun, B.L. Mordike, Laser produced functionally graded tungsten carbide coatings on M2 high-speed tool steel, *Materials Science & Engineering A (Structural Materials: Properties, Microstructure and Pro-cessing).* A302 (2001) 106-114.

[9] J. Tuominen, J., P. Vuoristo, T. Mantyla, M. Kylmalahti, J. Vihinen, P.H. Andersson, Improving corrosion properties of high-velocity oxy-fuel sprayed Inconel 625 by using a high-power continuous wave neodymium-doped yttrium aluminum garnet laser, *Journal of Thermal Spray Technology.* 9 (2000) 513-519.

[10] B.S. Yilbas, and B.J.A. Aleem, Dross formation during laser cutting process, *Journal of Applied Physics: Part D.* 39 (2006) 1451-1461.